AIMS Mathematics, 11(3): 7659–7686.
DOI: 10.3934/math.2026315
Received: 09 January 2026
Revised: 12 March 2026
Accepted: 19 March 2026
Published: 23 March 2026

https://www.aimspress.com/journal/Math

Research article

Dynamics of an SEIQHR-based mathematical model for infectious disease with awareness-driven optimal control

Khalid Aldawsari[1] **and Fahad Al Basir**[2,*]

[1] Department of Mathematics, College of Science and Humanities, Prince Sattam Bin Abdul Aziz University, Al-Kharj 11942, Saudi Arabia

[2] Department of Mathematics, Asansol Girls' College, Dr. Anjali Roy Sarani, Asansol-4, West Bengal 713304, India

* **Correspondence:** Email: fahadbasir@gmail.com, fahadalbasir@agc.ac.in; Tel: +03412257600.

Abstract: In this article, we extended the basic Susceptible-Exposed-Infectious-Quarantined-Hospitalized-Recovered (SEIQHR) compartmental model to the Susceptible-Exposed-Infectious-Quarantined-Hospitalized-Recovered-Awareness (SEIQHRA) framework by incorporating the level of awareness, A, as an additional model population to gain deeper insights into the dynamic process of infectious disease outbreaks, with particular emphasis on awareness-based interventions. Hospitalization, treatment, and quarantining procedures informed by awareness were integrated into this refined model. We investigated the key mathematical properties including boundedness of solutions, the basic reproduction number, and the existence of equilibriums. The model admitted two equilibria: The disease-free and the endemic equilibrium. The disease-free equilibrium was shown to be globally asymptotically stable when $R_0 < 1$ and unstable when $R_0 > 1$. Forward bifurcation occurred at $R_0 = 1$. The endemic equilibrium underwent a Hopf bifurcation, resulting in a stability switch. To design effective awareness-based interventions, the Pontryagin maximum principle was employed to derive optimal control parameters. Numerical simulations were conducted to validate the analytical findings, highlighting the role of awareness-driven control measures in controlling an infectious disease and enhancing public health outcomes.

Keywords: hospitalization; basic reproduction number; stability analysis; forward and hopf bifurcation analysis; bubbling dynamics; optimal control problem; numerical simulations
Mathematics Subject Classification: 92-10, 34C23, 49J15

1. Introduction

Infectious diseases, caused by pathogenic microorganisms involving viruses, bacteria, fungi, and parasites, continue to raise daunting challenges to global health [1]. The Kingdom of Saudi Arabia was not immune to the rising tide of infectious diseases, which resulted in the emergence of massive epidemics such as Middle East Respiratory Syndrome (MERS) in 2012, caused by a novel coronavirus, claiming over 2,000 cases with a substantial death toll [2], and the COVID-19 pandemic in 2020, with over 500,000 confirmed cases with a substantial death toll within the mid-period of 2021 [3]. The camel-sourced MERS was contained after intensive public health awareness campaigns were conducted by the Saudi Ministry of Health, engaging the entire population on the need for proper personal, animal, and healthcare-related infection control [4, 5]. The Saudi government implemented a far-reaching control program for the massive COVID-19 pandemic, involving suspended mass gatherings for Umrah and Hajj, wearing masks, maintaining a safe distance, and promoting COVID-19 vaccinations through multi-language broadcasting [6]. The Saudi government passed amended laws for supportive quarantine measures, coordinating measures for responding to emergencies, with the engagement of the Saudi Religious leaders to supress the call for public gatherings [7]. Among the most effective tools for understanding the mechanisms of disease transmission, predicting outbreak trajectories, and evaluating the impact of intervention strategies is mathematical modeling [26].

During the period of observation, there has been a marked decrease in the reported cases of two serious contagious diseases, Tuberculosis (TB) and Hepatitis B, which is an indication of marked success in efforts to promote public health. The reported incidence of TB has steadily reduced from 3,500 to 2,100, which is a decline of 40% and is an indication of marked success in screening programs, treatment, and community education efforts [8]. The reported incidence of Hepatitis B has also reduced from 4,200 to 2,800, which is a decline of 33% and can be attributed to marked success in vaccination and screening programs, as well as community awareness programs regarding preventive measures [9].

Hence, we identify the importance of awareness programs regarding the dynamics and prevention of diseases. The basic modeling approach within this context is the SIR (Susceptible, Infectious, Recovered) based deterministic model, which was first conceptualized for analyzing past pandemic diseases [16, 19]. Since the conceptualization of the SIR based approach, the model has remained the foundation for epidemiological modeling, which has advanced to account for the intricacies of the transmission process, heterogeneity, acquired immunity, along with the applications of various interventions like vaccinations, quarantines, and hospitalizations. However, to further enhance modeling within this context, the SEIQR (Susceptible–Exposed–Infectious–Quarantined–Recovered) approach provides a more refined mechanism of modeling based on the dynamics relating to control measures [10]. The introduction of a quarantined category within the approach helps to enhance the existing Susceptible–Exposed–Infectious–Recovered (SEIR) based mechanism for capturing the relevance of early detection, tracing, and isolation procedures [20]. The population is categorized into five compartments: susceptible individuals at risk of infection; exposed individuals in the incubation phase; infectious individuals capable of transmitting the disease; quarantined individuals isolated to prevent further spread; and recovered individuals who have acquired immunity [35].

The Susceptible-Infected-Quarantined-Recovered (SIQR) model helps in performing calculations for important epidemiological parameters such as the dynamics of the disease and its control [30].

Recent studies demonstrate the importance of SEIQR models for evaluating non-pharmaceutical interventions and resource allocation in health crises [34]. For instance, Kao et al. [21] used the concept of reinforcement learning coupled with semi-connected SEIQR models for pandemic control in various regions, maintaining a balance between epidemiological and economic factors. In a similar study, Younsi et al. [22] proposed a spatial decision-support system for understanding the spread of COVID-19 on scale-free networks, following SEIQR dynamics. In the SEIQHR model, the E (Exposed) class represents individuals who are infected but not yet infectious, capturing the latent period before they become contagious. This is crucial for diseases with incubation phases, such as COVID-19 or Hepatitis E, because it accounts for the delay in transmission and helps predict outbreak timing and spread more accurately. The H (Hospitalized) class represents severe cases that require medical care. It helps estimate healthcare demand such as hospital beds and ICU capacity, distinguishes mild from severe infections, and is critical for pandemic policy planning by anticipating resource needs and guiding intervention strategies [25]. Awareness campaigns have impacts on the populations and transmission process. Thus we propose here an SEIQHR based model with awareness effects by assuming the transmission rates as function of awareness level, A.

To extend the SEIQR model or SEIQHR model (Susceptible, Exposed, Infectious, Quarantined, Recovered) in [14, 15, 23, 24], an extra compartment A is included to derive the SEIQHRA model. The new version helps understand the effect of the health care system capacity, as done for diseases with high health care burden. In the extended SEIQHR model, we use the influence of awareness-based interventions and campaigns and assumed the transition rates of the disease as the function of 'level of awareness', $A(t)$ at any time t. For this study, the SEIQHR-based model with effects of awareness campaigns is proposed for the assessment of epidemiological thresholds and stability analysis, its ability for simulating these aspects for decision-making. Dynamics behaviors such as stability of equilibrium, and Basic reproduction number are important for this analysis [13]. Hopf Bifurcation is another aspect of this study for analysis of the periodic dynamics of the infectious disease model around the endemic equilibria [13]. Optimization is another aspect which is also essential for the development of intervention plans that balance control of the disease and resource limitations [11].

Optimal control strategies using vaccination, treatment, and social distancing etc., have been effectively integrated into these models to manage epidemic dynamics [17]. By leveraging Pontryagin's Maximum Principle, researchers can derive time-dependent control functions that inform public health policies under constrained resources [18]. Recent applications of optimal control in SEIQHR-type models, particularly in the context of COVID-19, have demonstrated that well-timed interventions can significantly reduce peak infection rates and alleviate pressure on healthcare systems [15, 23]. In the proposed model, we applied the optimal control approach to minimize the cost of disease management by finding optimal rate of awareness campaigns, treatment, and hospitalization.

The aim of this paper is the incorporation of awareness as an additional dynamic compartment into the SEIQHR framework and arriving at the SEIQHRA model. Though various SEIQHR models have studied quarantine, recovery, and healthcare capacity in the past, none have focused on the incorporation of awareness-based interventions into the transmission dynamics. The novelty of this study is in providing a new perspective to analyze the quantification of awareness-based interventions and their impact on disease thresholds, stability conditions, and bifurcations. In our knowledge, the incorporation of awareness into the mathematical structure of the SEIQHR model is the novelty of this paper. It provides a unique contribution to the quantification and evaluation of awareness-based

interventions in the context of infectious disease dynamics.

In this study, we introduce a novel mathematical model based on the SEIQHR framework to examine infectious disease dynamics under the influence of awareness campaigns. In the model, media awareness–represented as $A(t)$– is treated as a population variable, with transmission rates expressed as functions of $A(t)$. A central objective of the work is to design an optimal control strategy that reduces infection levels through awareness-driven interventions. Fundamental aspects of mathematical modeling such as equilibrium states, the basic reproduction number, and the stability of equilibria are explored using analytical and qualitative methods. Additionally, the endemic equilibrium is investigated through Hopf bifurcation analysis. The optimal control problem, incorporating three distinct control parameters, is addressed via the maximum principle. Finally, numerical simulations carried out in MATLAB validate the theoretical findings.

2. Formulation of the model

The SEIQHR model is a compartmental framework designed to capture the progression and control of infectious diseases within a population. It stratifies individuals into six dynamic compartments, namely, the following

$S(t)$: Susceptible individuals who are at risk of contracting the disease,
$E(t)$: Exposed individuals who have been infected but are not yet infectious,
$I(t)$: Infectious individuals capable of transmitting the disease,
$Q(t)$: Quarantined individuals isolated to prevent further spread,
$H(t)$: Hospitalized individuals receiving medical treatment due to severe symptoms,
$R(t)$: Recovered individuals assumed to have acquired immunity.

Individuals enter the susceptible class (S) at a constant recruitment rate Π, representing population inflow through birth or immigration. They interact at a rate λ with the infected population and join the exposed class. Exposed individuals (E) transition to the infectious class at rate μ, marking the onset of symptoms and transmission potential.

Infectious individuals (I) can progress along one of the following courses of illness. These individuals can be quarantined at a rate of q, or they may recover at a rate of r_1, or they may die from the disease at a rate of δ, reflecting mortality from the disease. When quarantined (Q), these individuals can proceed to hospitalization at a rate of h, or they can get cured at a rate of r_2, or they may die from the disease at the same rate δ. For individuals who are already hospitalized (H), there are two possibilities for their future course of illness. These are recovering at a rate of r_3, or dying from the disease at the same rate of δ. The recovered persons (R) are assumed to gain immunity for their lifetime, thus leaving the replication cycle forever. In other words, the recovered persons will not be re-infected.

All categories, Susceptible, Exposed, Infectious, Quarantined, Hospitalized, and Recovered, are prone to natural or ordinary mortality at a constant rate d. On the other hand, mortality rate δ caused by the disease is exclusively among the Infectious, Quarantined, and Hospitalized individuals, adding to the cumulative number of disease-related deaths.

We now impose the impact of awareness campaigns in the following manner. To account for the influence of public information dissemination and media-driven behavioral responses, we introduce

an auxiliary variable $A(t)$, representing the level of awareness within the population. This variable plays a pivotal role in modulating both the transmission dynamics and the transition rates between epidemiological compartments. The following hypotheses are introduced.

H1: The force of infection is attenuated by awareness through a nonlinear incidence function:

$$\frac{\lambda S I}{1 + cA},$$

where λ denotes the baseline transmission rate in the absence of awareness, and c is a saturation constant that quantifies the diminishing marginal effect of increasing awareness.

H2: The rates of quarantine, recovery, and hospitalization are assumed to be proportional to the prevailing awareness level. Specifically, the quarantine rate becomes qA, the recovery rates for infected, quarantined, and hospitalized individuals become r_1A, r_2A, and r_3A, respectively, and the hospitalization rate becomes hA. These modifications reflect enhanced responsiveness and intervention efficacy under heightened public awareness.

H3: The evolution of awareness is governed by the differential equation:

$$\frac{dA}{dt} = \omega + \gamma(I + Q + H) - \theta A,$$

where ω represents the increase in awareness level due to global sources such as social media, and γ captures the contribution from local sources which is proportional to the total number of infected, quarantined, and hospitalized individuals, and θ denotes the rate of awareness decay due to the loss of public interest.

Incorporating these effects, the complete SEIQHRA model is formulated as follows:

$$\begin{aligned}
\frac{dS}{dt} &= \Pi - \frac{\lambda S I}{1 + cA} - dS, \\
\frac{dE}{dt} &= \frac{\lambda S I}{1 + cA} - \mu E - dE, \\
\frac{dI}{dt} &= \mu E - (d + \delta + qA + r_1A)I, \\
\frac{dQ}{dt} &= qIA - (d + \delta)Q - hQA - r_2QA, \\
\frac{dH}{dt} &= hQA - (d + \delta)H - r_3HA, \\
\frac{dR}{dt} &= r_1IA + r_2QA + r_3HA - dR, \\
\frac{dA}{dt} &= \omega + \gamma(I + Q + H) - \theta A.
\end{aligned} \tag{1}$$

The initial population sizes are

$$S(0) \geq 0, \quad E(0) \geq 0, \quad I(0) \geq 0, \quad Q(0) \geq 0, \quad H(0) \geq 0, \quad R(0) \geq 0, \quad A(0) \geq 0. \tag{2}$$

The mechanism mentioned above is shown in Figure 1 using a flow diagram. A brief description of the parameters is provided in Table 1.

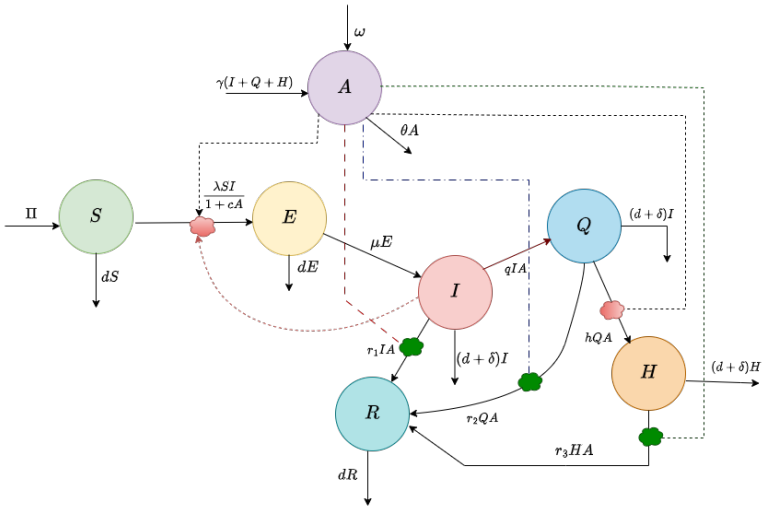

Figure 1. Schismatic flow diagram of the model (1).

Table 1. Description and values of model parameters [30, 33, 38, 39].

Parameter	Description	Value (unit)
Π	Recruitment rate of susceptible population	40 individuals day^{-1}
d	Natural death rate of human population	0.01 day^{-1}
λ	Transmission rate of the disease	0.000025 individual^{-1}day^{-1}
c	Saturation constant for media awareness effect	0.5 (dimensionless)
μ	Rate at which exposed individuals become infectious	0.15 day^{-1}
δ	Disease-induced death rate	0.01 day^{-1}
q	Quarantine rate of infected individuals	0.02 day^{-1}
r_1	Recovery rate of infectious individuals	0.002 day^{-1}
h	Hospitalization rate of quarantined individuals	0.03 day^{-1}
r_2	Recovery rate of quarantined individuals	0.023 day^{-1}
r_3	Recovery rate of hospitalized individuals	0.02 day^{-1}
ω	Awareness increase rate by global sources (TV, social media, etc.)	0.003 day^{-1}
γ	Awareness increase due to local factors	0.0025 individual^{-1}day^{-1}
θ	Rate of decay or loss of media awareness	0.015 day^{-1}

3. Basic properties of the model

In this part, we examine the essential attributes of the system, focusing on the boundedness of solutions, the determination of equilibrium states, and the derivation of the basic reproduction number. Such investigations confirm both the biological plausibility and the mathematical soundness of the model.

3.1. Boundedness

The following theorem establishes the nonnegativity and boundedness of solutions.

Theorem 1. *Solutions of the system* (1) *with initial condition* (2) *are nonnegativity and bounded for all* $t > 0$.

Thus, we have the following result on the boundedness of solutions of system (1).

Theorem 2. *All solutions of system* (1) *are bounded in the region* $\mathcal{B}$ *where*

$$\mathcal{B} = \left\{(S, E, I, Q, H, R, A) \in \mathbb{R}^7 : 0 \leq S + E + I + Q + H + R \leq \frac{\Pi}{d},\ 0 \leq A(t) \leq \frac{\omega d + \gamma\Pi}{d\theta}\right\}. \tag{3}$$

Proof. Let the total population be:

$$N(t) = S(t) + E(t) + I(t) + Q(t) + H(t) + R(t).$$

We compute $\frac{dN}{dt}$ by summing the first six equations:

$$\frac{dN}{dt} = \Pi - dN - \delta(I + Q + H) \leq \Pi - dN. \tag{4}$$

Solving this differential inequality, we get

$$\limsup_{t\to\infty} N(t) = \frac{\Pi}{d}. \tag{5}$$

This shows that $N(t)$ is bounded above by $\frac{\Pi}{d}$ for all $t > 0$. Again, from the last equation of system (1), we can write

$$\frac{dA}{dt} = \omega + \gamma(I + Q + H) - \theta A.$$

Since $N(t) \leq \frac{\Pi}{d}$, we get:

$$\frac{dA}{dt} \leq \omega + \frac{\gamma\Pi}{d} - \theta A.$$

Using the framework of functional differential equations, we obtain

$$\limsup_{t\to\infty} A(t) = \frac{\omega d + \gamma\Pi}{d\theta}. \tag{6}$$

Hence, $A(t)$ remains bounded for all $t > 0$. Consequently, every solution originating from $\mathcal{B}$ stays within this set for all $t > 0$. □

3.2. Equilibria

This sections contains the equilibria, characteristic equation, and stability analysis of equilibria.

3.3. Existence of equilibria

The system has two equilibria, namely,

(i) the disease-free equilibrium (DFE), $E_0\left(\frac{\Pi}{d}, 0, 0, 0, 0, 0, \frac{\omega}{\theta}\right)$,

(ii) the endemic equilibrium $E^*(S^*, I^*, Q^*, H^*, R^*, P^*, M^*)$, where

$$S^* = \frac{(1 + cA^*)(\mu + d)(d + \delta + qA^* + r_1A^*)}{\mu\lambda},$$

$$
\begin{aligned}
I^* &= \frac{\mu(\Pi - dS^*)}{(1 + cA^*)(\mu + d)(d + \delta + qA^* + r_1A^*)},\\
Q^* &= \frac{qA^*I^*}{d + \delta + hA^* + r_2A^*},\\
H^* &= \frac{hqA^{*2}I^*}{(d + \delta + hA^* + r_2A^*)(d + \delta + r_3A^*)},\\
R^* &= \frac{A^*}{d}\left[r_1I^* + r_2Q^* + r_3H^*\right],
\end{aligned}
$$

where A^* satisfies the following cubic equation:

$$P_3A^3 + P_2A^2 + P_1A + P_0 = 0 \tag{7}$$

with coefficients:

$$
\begin{aligned}
P_3 &= -\theta + \frac{\gamma\mu^2\Pi qh}{\lambda(d + \delta)^2(\mu + d)},\\
P_2 &= \frac{\gamma\mu^2\Pi q}{\lambda(d + \delta)(\mu + d)} + \frac{\gamma\mu^2\Pi qh(r_2 + r_3)}{\lambda(d + \delta)^2(\mu + d)},\\
P_1 &= \frac{\gamma\mu^2\Pi}{\lambda(\mu + d)} + \frac{\gamma\mu^2\Pi q(r_2 + r_3)}{\lambda(d + \delta)(\mu + d)} - \frac{\gamma d(1 + q + qh)}{\lambda},\\
P_0 &= \omega - \frac{\gamma dqh}{\lambda}.
\end{aligned}
$$

Equation (7) is a cubic polynomial, thus there exists a real root of this equation. If P_3 and P_0 have an opposite sign, then one feasible endemic equilibrium is possible. Also, I^* is positive when $dS^* < \Pi$.

Existence condition. (i) DFE E_0 always exists, (ii) E^* exists when $dS^* < \Pi$ and P_3 and P_0 are of opposite sign.

3.4. Basic reproduction number

The basic reproduction number is derived through the next generation matrix approach. The matrix G is constructed from two components, **F** and **V**. Here, **F** denotes the matrix of new infections (transmission), while **V** represents the matrix of transitions among infected compartments.

Let **f** denote the vector of transmission terms from infected to susceptible classes, and let **v** denote the vector of transition rates among infected compartments.

The Jacobian matrices of **f** and **v** are represented by **F** and **V**, respectively. Each entry of **F**, F_{ij}, corresponds to the partial derivative $F_{ij} = \frac{\partial f_i}{\partial x_j}$, where f_i is the i^{th} component of **f** and x_j is the j^{th} infected variable.

Similarly, the entries of **V** are given by $V_{ij} = \frac{\partial v_i}{\partial x_j}$, where v_i is the i^{th} component of **v** and x_j is the j^{th} infected variable.

The vectors **f** and **v** must include the infected class I, corresponding to the compartmental structure defined in Eq (1). Thus, we obtain:

$$\mathbf{f} = \begin{pmatrix} \frac{\lambda SI}{1+cA} \\ 0 \end{pmatrix}, \quad \mathbf{v} = \begin{pmatrix} (\mu + d)E \\ -\mu E + (d + \delta + qA + r_1A)I \end{pmatrix}. \tag{8}$$

From the above matrices, we derive

$$F = \begin{pmatrix} 0 & \frac{\lambda\Pi}{d(1+cA)} \\ 0 & 0 \end{pmatrix}$$

and

$$V = \begin{pmatrix} \mu + d & 0 \\ -\mu & d + \delta + qA + r_1 A \end{pmatrix}.$$

The basic reproduction number $\mathcal{R}_0$ is the dominant eigenvalue of the matrix $G(E_0) = FV^{-1}$, where E_0 is the DFE. We cancellate the next generation matrix as

$$G = \frac{1}{(\mu + d)(d + \delta + qA + r_1 A)} \begin{pmatrix} \frac{\lambda\Pi\mu}{d(1+cA)} & \frac{\lambda\Pi(\mu+d)}{d(1+cA)} \\ 0 & 0 \end{pmatrix}.$$

We find the basic reproduction number as

$$R_0 = \frac{\lambda\Pi\mu}{d(1 + cA_0)(\mu + d)(d + \delta + qA_0 + r_1 A_0)}, \tag{9}$$

and this is the largest eigenvalue of G and $A_0 = \frac{\omega}{\theta}$ (the steady state value of $A(t)$ at DFE). Using $A_0 = \frac{\omega}{\theta}$, the final expression for R_0 is given below:

$$R_0 = \frac{\lambda\Pi\mu\theta}{d(\theta + c\omega)(\mu + d)\,(\theta d + \theta\delta + (q + r_1)\omega)} \tag{10}$$

Remark 1. *Detail numerical simulations show that endemic equilibrium E^* exists when $R_0 > 1$ (for example, see Figure 2).*

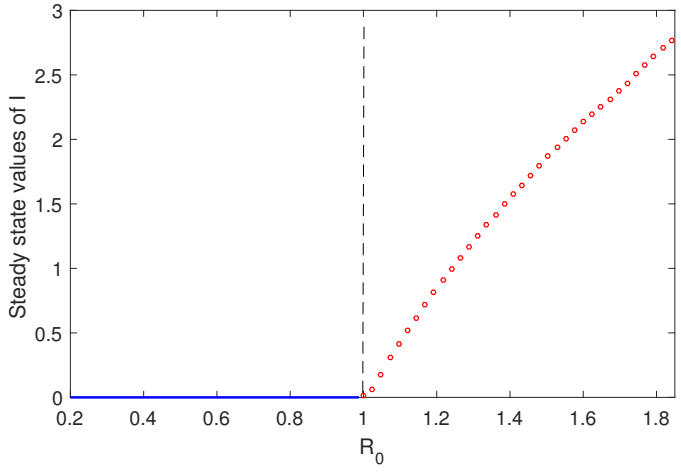

Figure 2. Forward bifurcation: Steady state values of infected population are plotted. Here infection rate λ is varied. Rest of the parameter values are taken from Table 1.

4. Stability of equilibria

Here, we have studied the stability of equilibria by finding the nature of eigenvalues of the Jacobian matrix at each equilibrium point.

4.1. Stability of DFE

The Jacobian matrix at the DFE is given by

$$J_{\text{DFE}} = \begin{bmatrix} -d & 0 & -\frac{\lambda\Pi}{d(1+cA_0)} & 0 & 0 & 0 & 0 \\ 0 & -(\mu+d) & \frac{\lambda\Pi}{d(1+cA_0)} & 0 & 0 & 0 & 0 \\ 0 & \mu & -(d+\delta+\alpha_1) & 0 & 0 & 0 & 0 \\ 0 & 0 & \alpha_2 & -(d+\delta+\alpha_3) & 0 & 0 & 0 \\ 0 & 0 & 0 & \alpha_4 & -(d+\delta+\alpha_5) & 0 & 0 \\ 0 & 0 & \alpha_6 & \alpha_7 & \alpha_8 & -d & 0 \\ 0 & 0 & \gamma & \gamma & \gamma & 0 & -\theta \end{bmatrix},$$

where, $\alpha_1 = \frac{\omega}{\theta}(q + r_1)$, $\alpha_2 = q\frac{\omega}{\theta}$, $\alpha_3 = \frac{\omega}{\theta}(h + r_2)$, $\alpha_4 = h\frac{\omega}{\theta}$, $\alpha_5 = r_3\frac{\omega}{\theta}$, $\alpha_6 = r_1\frac{\omega}{\theta}$, $\alpha_7 = r_2\frac{\omega}{\theta}$, and $\alpha_8 = r_3\frac{\omega}{\theta}$. Five eigenvalues are negative and the remaining two eigenvalues satisfy

$$x^2 + (\mu + 2d + \delta + \alpha_1)x + (\mu + d)(d + \delta + \alpha_1) - \frac{\mu\lambda\Pi}{d(1 + cA_0)} = 0. \tag{11}$$

Using (9), we rewrite (11) as

$$x^2 + (\mu + 2d + \delta + \alpha_1)x + (\mu + d)(d + \delta + \alpha_1)(1 - R_0) = 0. \tag{12}$$

The roots of (12) are negative if the constant term of this equation is positive, i.e., when $R_0 < 1$. Thus DFE is stable when $R_0 < 1$.

4.2. Forward bifurcation analysis

We have the following theorem for characterizing the bifurcation at $R_0 = 1$.

Theorem 3. *(i) If $R_0 < 1$, the DFE is locally asymptotically stable,*
(ii) if $R_0 > 1$, the DFE becomes unstable, and
(iii) at $R_0 = 1$, the system undergoes a forward (supercritical) transcritical bifurcation.

Proof. To analyze the bifurcation at $R_0 = 1$, we apply the method developed by Castillo-Chavez and Song (2004), which uses center manifold theory to determine the direction and type of bifurcation. The system is partitioned into infected compartments $x = (E, I, Q, H)$ and uninfected compartments $y = (S, R, A)$, with the transmission rate λ treated as the bifurcation parameter.

At the DFE E_0, the Jacobian matrix of the infection subsystem is given by

$$J = \begin{pmatrix} -(\mu + d) & \beta & 0 & 0 \\ \mu & -\alpha_1 & 0 & 0 \\ 0 & qA_0 & -\alpha_2 & 0 \\ 0 & 0 & hA_0 & -\alpha_3 \end{pmatrix},$$

where $\beta = \dfrac{\lambda\Pi}{d(1 + \frac{c\omega}{\theta})}$, $A_0 = \dfrac{\omega}{\theta}$, and

$$\alpha_1 = d + \delta + \frac{(q + r_1)\omega}{\theta}, \quad \alpha_2 = d + \delta + \frac{(h + r_2)\omega}{\theta}, \quad \alpha_3 = d + \delta + \frac{r_3\omega}{\theta}.$$

At the value $R_0 = 1$, the Jacobian matrix has a simple zero eigenvalue. Let $w = (w_1, w_2, w_3, w_4)^T$ be the right eigenvector corresponding to this eigenvalue. Setting $w_2 = 1$, we obtain

$$w_1 = \frac{\beta}{\mu + d}, \quad w_3 = \frac{qA_0}{\alpha_2}, \quad w_4 = \frac{hA_0 \cdot qA_0}{\alpha_2\alpha_3}.$$

Let us write by $v = (v_1, v_2, v_3, v_4)$ the left eigenvector of J, normalized such that $v \cdot w = 1$. On setting $v_2 = 1$, we get

$$v_1 = \frac{\mu}{\mu + d}, \quad v_3 = \frac{\alpha_1}{qA_0}, \quad v_4 = \frac{\alpha_1\alpha_2}{qh(A_0)^2}.$$

The normalization factor is the following:

$$\Sigma = v \cdot w = \frac{\mu\beta}{(\mu + d)^2} + 1 + \frac{\alpha_1}{\alpha_2} + \frac{\alpha_1}{\alpha_3},$$

thus, the normalized left eigenvector is given by:

$$v = \frac{1}{\Sigma} \cdot \left(\frac{\mu}{\mu + d}, \ 1, \ \frac{\alpha_1}{qA_0}, \ \frac{\alpha_1\alpha_2}{qh(A_0)^2} \right).$$

To compute the bifurcation coefficients, we note that the only nonlinear term in the infection subsystem is $f_1 = \frac{\lambda S I}{1+cA}$. The mixed partial derivative evaluated at the DFE is

$$\left.\frac{\partial^2 f_1}{\partial I \partial A}\right|_{DFE} = -\frac{\lambda S c}{(1 + cA)^2} = -\frac{\lambda \Pi c}{d(1 + \frac{c\omega}{\theta})^2}.$$

Thus, the bifurcation coefficient a is given by

$$a = v_1 w_2 \cdot \left(-\frac{\lambda \Pi c}{d(1 + \frac{c\omega}{\theta})^2} \right) = -\frac{1}{\Sigma} \cdot \frac{\mu}{\mu + d} \cdot \frac{\lambda \Pi c}{d(1 + \frac{c\omega}{\theta})^2}.$$

Similarly, the sensitivity coefficient b is computed from

$$\left.\frac{\partial^2 f_1}{\partial I \partial \lambda}\right|_{DFE} = \frac{S}{1 + cA} = \frac{\Pi}{d(1 + \frac{c\omega}{\theta})},$$

which gives

$$b = v_1 w_2 \cdot \frac{\Pi}{d(1 + \frac{c\omega}{\theta})} = \frac{1}{\Sigma} \cdot \frac{\mu}{\mu + d} \cdot \frac{\Pi}{d(1 + \frac{c\omega}{\theta})}.$$

Since all model parameters are positive, it follows that $a < 0$ and $b > 0$. Therefore, by the theorem of Castillo-Chavez and Song (2004) [28], the system undergoes a forward (supercritical) transcritical bifurcation at $R_0 = 1$, and a unique endemic equilibrium emerges for $R_0 > 1$. □

4.3. Global stability of the DFE

Theorem 4. *If the basic reproduction number*

$$R_0 = \frac{\lambda \Pi}{d\left(1 + \frac{c\omega}{\theta}\right)} \cdot \frac{\mu}{(\mu + d)\left(d + \delta + \frac{\omega}{\theta}(q + r_1)\right)},$$

satisfies $R_0 < 1$, then the DFE is globally asymptotically stable.

Proof. Define the Lyapunov function:

$$\mathcal{L}(t) = E(t) + \frac{\mu}{\beta(t)} I(t),$$

where $\beta(t) = d + \delta + A(t)(q + r_1)$. Since $A(t) \geq 0$, we have $\beta(t) > 0$, ensuring that $\mathcal{L}(t)$ is positive definite and differentiable.

Differentiating $\mathcal{L}(t)$ with respect to time:

$$\frac{d\mathcal{L}}{dt} = \frac{dE}{dt} + \frac{\mu}{\beta(t)} \frac{dI}{dt} - \frac{\mu\beta'(t)}{\beta(t)^2} I(t).$$

Substituting the model equations:

$$\frac{dE}{dt} = \frac{\lambda S I}{1 + cA} - (\mu + d)E, \quad \frac{dI}{dt} = \mu E - \beta(t)I,$$

we obtain:

$$\frac{d\mathcal{L}}{dt} = \left(\frac{\lambda S}{1 + cA} - \mu\right) I - dE - \frac{\mu\beta'(t)}{\beta(t)^2} I.$$

Now, since $S \leq \frac{\Pi}{d}$, we estimate:

$$\frac{\lambda S}{1 + cA} \leq \frac{\lambda \Pi}{d(1 + cA)}.$$

Also, since

$$\beta'(t) = (q + r_1)(\omega + \gamma(I + Q + H) - \theta A),$$

we have

$$\beta'(t) \leq (q + r_1)(\omega + \gamma(I + Q + H)) \Rightarrow \frac{\mu\beta'(t)}{\beta(t)^2} I \geq 0.$$

Thus,

$$\frac{d\mathcal{L}}{dt} \leq \left(\frac{\lambda \Pi}{d(1 + cA)} - \mu\right) I - dE.$$

At the DFE, $A = \frac{\omega}{\theta}$, so the condition $R_0 < 1$ implies:

$$\frac{\lambda \Pi}{d(1 + \frac{c\omega}{\theta})} < \mu \cdot \frac{(\mu + d)}{d + \delta + \frac{\omega}{\theta}(q + r_1)}.$$

This ensures:

$$\frac{\lambda \Pi}{d(1 + cA)} < \mu \quad \text{for all } A(t) \geq 0,$$

and, therefore:

$$\frac{d\mathcal{L}}{dt} < 0 \quad \text{whenever } E > 0 \text{ or } I > 0.$$

Since $\mathcal{L}(t)$ is positive definite and radially unbounded, and $\frac{d\mathcal{L}}{dt} \leq 0$ with equality only at the DFE, LaSalle's invariance principle implies that the DFE is globally asymptotically stable. □

5. Stability of endemic equilibrium

The Jacobian matrix in this case is

$$J = [J_{ij}]_{7\times 7} = \begin{bmatrix} J_{11} & 0 & -\frac{\lambda S}{1+cA} & 0 & 0 & 0 & \frac{\lambda S Ic}{(1+cA)^2} \\ \frac{\lambda I}{1+cA} & -(\mu+d) & \frac{\lambda S}{1+cA} & 0 & 0 & 0 & -\frac{\lambda S Ic}{(1+cA)^2} \\ 0 & \mu & J_{33} & 0 & 0 & 0 & -(q+r_1)I \\ 0 & 0 & qA & J_{44} & 0 & 0 & qI-(h+r_2)Q \\ 0 & 0 & 0 & hA & -(d+\delta+r_3A) & 0 & hQ-r_3H \\ 0 & 0 & r_1A & r_2A & r_3A & -d & r_1I+r_2Q+r_3H \\ 0 & 0 & \gamma & \gamma & \gamma & 0 & -\theta \end{bmatrix},$$

where, $J_{11} = -\frac{\lambda I}{1+cA} - d$, $J_{33} = -(d+\delta+A(q+r_1))$, $J_{44} = -(d+\delta+A(h+r_2))$.

The characteristic equation in x is obtained as

$$h(x) = (x+d)(x^6 + J_1x^5 + J_2x^4 + J_3x^3 + J_4x^2 + J_5x + J_6) = 0. \tag{13}$$

The coefficients of (13) are given in Appendix A.

According to the Routh–Hurwitz stability criteria, the characteristic Eq (13) will possess roots with negative real parts provided the following conditions are met:

$$\begin{aligned} &i)\ J_i > 0,\ i = 1, 2, ..., 6, \\ &ii)\ J_1J_2 - J_3 > 0, \\ &iii)\ J_3(J_1J_2 - J_3) - J_1(J_1J_4 - J_5) > 0, \\ &iv)\ J_1J_2J_3J_4 - J_3^2J_4 - J_1^2J_4^2 - J_1J_2^2J_5 + J_2J_3J_5 + 2J_1J_4J_5 - J_5^2 + J_1^2J_2J_6 - J_1J_3J_6 > 0, \\ &v)\ J_1J_2J_3J_4J_5 - J_3^2J_4J_5 - J_1^2J_4^2J_5 - J_1J_2^2J_5^2 + J_2J_3J_5^2 + 2J_1J_4J_5^2 - J_5^3 \\ &\quad - J_1J_2J_3^2J_6 + J_3^3J_6 + J_1^2J_3J_4J_6 + 2J_1^2J_2J_3J_6 - 3J_1J_3J_5J_6 - J_1^3J_6^2 > 0. \end{aligned} \tag{14}$$

Now, we study if there is any stability switch in the system. Hopf bifurcation refers to a situation where a fixed point of a dynamical system loses stability as a parameter is varied, leading to the emergence of a periodic solution (limit cycle). For a 6-dimensional system, the existence of a Hopf bifurcation can be determined by analyzing the eigenvalues of the system's Jacobian matrix evaluated at the fixed point. We use the following theorem established in [27] to study the Hopf bifurcation in the system:

Theorem 5. *The endemic equilibrium E^* undergoes a Hopf bifurcation corresponding to the generic bifurcation parameter ζ at ζ^*, if the following conditions are satisfied:*

i) $J_i(\zeta^*) > 0, \quad \forall i = 1, 2, \ldots, 6,$

ii) $[J_1J_2 - J_3]_{\zeta=\zeta^*} = 0,$

iii) $[J_1J_2J_3 - J_1^2J_4 - J_3^2 - J_5]_{\zeta=\zeta^*} = 0,$

iv) $\left[(J_1J_2 - J_3)(J_3^2 - J_1^2J_4 + J_5) + (J_1J_2 - J_3)(J_1J_6 - J_1^2J_5)\right]_{\zeta=\zeta^*} = 0,$

v) $[H_5]_{\zeta=\zeta^*} = \Big[J_1J_2J_3J_4 - (J_1J_2 - J_3)\Big(J_4J_5J_6 + J_3J_6(J_2J_5 - J_1J_6) + J_1J_2J_6^2 - 2J_1J_2J_6^2J_1J_6^2 - J_5(J_1J_4 - J_2J_3)\Big)\Big]_{\zeta=\zeta^*} = 0,$

vi) *Transversality condition given below should be satisfied:*

$$\frac{1}{M_6}\left[\frac{dH_5}{d\zeta}\right]_{\zeta=\zeta^*} \neq 0,$$

where

$$M_6 = 2J_1(J_1J_4 - J_5) - J_3(J_1J_2 - J_3) \cdot \begin{vmatrix} -J_1 & 1 & 1 & 0 & 0 \\ J_2 - 2\phi & -J_1 & 0 & 1 & 0 \\ J_1\phi - J_3 & J_2 - \phi & 0 & 1 & 1 \\ \phi^2 - J_2\phi + J_4 & 0 & \phi & 0 & \phi \\ 0 & \phi^2 - J_2\phi + J_4 & 0 & 0 & \phi \end{vmatrix},$$

with

$$\phi = \frac{J_3J_5 + J_1^2J_6 - J_1J_2J_5}{J_1^2J_4 - J_1J_3 - J_1J_2J_3 + J_3^2}.$$

6. Sensitivity analysis

The individual sensitivity indices for each parameter in the basic reproduction number R_0, based on the formula:

$$\Gamma_x^{R_0} = \frac{\partial R_0}{\partial x} \cdot \frac{x}{R_0}. \tag{15}$$

Using the expression in (15), the sensitivity indices for each parameter are calculated and presented in Table 2.

These expressions give the sensitivity index for each parameter. We use the baseline parameter values of the parameters from Table 1 to plot the sensitivity indices.

From the simulations, we found the most sensitive parameters affecting R_0 are the natural death rate d, baseline death input ω, recruitment rate Π, and transmission rate λ. These have the largest impact on the basic reproduction number.

Highly sensitive parameters include d, ω, Π, and λ. The natural death rate d appears in multiple denominator terms, amplifying its effect. The baseline death input ω influences both awareness and disease burden. Recruitment rate Π and transmission rate λ directly scale the numerator, making them proportionally impacted.

Moderately sensitive parameters such as c, δ, q, and r_1 affect awareness and recovery dynamics. Least sensitive parameters include μ and θ, whose influence is dampened by their presence in both the numerator and denominator.

Table 2. Expression for sensitivity indices of parameters with respect to R_0 and their numeric value for the parameters as in Table 1.

Parameter	Expression for sensitivity	Sensitivity values
λ	1	1
Π	1	1
μ	$1-\frac{\mu}{\mu+d}$	0.063
θ	$1-\frac{\theta}{\theta+c\omega}-\frac{\theta d+\theta\delta}{\theta d+\theta\delta+(q+r_1)\omega}$	−0.776
d	$-1-\frac{d}{\mu+d}-\frac{\theta d}{\theta d+\theta\delta+(q+r_1)\omega}$	−1.496
c	$-\frac{c\omega}{\theta+c\omega}$	−0.091
ω	$-\frac{c\omega}{\theta+c\omega}-\frac{(q+r_1)\omega}{\theta d+\theta\delta+(q+r_1)\omega}$	−0.282
δ	$-\frac{\theta\delta}{\theta d+\theta\delta+(q+r_1)\omega}$	−0.434
q	$-\frac{q\omega}{\theta d+\theta\delta+(q+r_1)\omega}$	−0.173
r_1	$-\frac{r_1\omega}{\theta d+\theta\delta+(q+r_1)\omega}$	−0.017

7. The optimal control problem

We aim here to control the hospitalization rate h, quarantine rate q, and awareness campaigns rate ω. For this, two parameters $u_i, i = 1, 2, 3$, are introduced in the model to obtain the following state system:

$$\begin{aligned}
\frac{dS}{dt} &= \Pi-\frac{\lambda SI}{1+A}-dS,\\
\frac{dE}{dt} &= \frac{\lambda SI}{1+A}-\mu E-dE,\\
\frac{dI}{dt} &= \mu E-(d+\delta+qA+u_1r_1A)I,\\
\frac{dQ}{dt} &= qIA-(d+\delta)Q-u_2hQA-u_1r_2QA,\\
\frac{dH}{dt} &= u_2hQA-(d+\delta)H-u1r_3HA,\\
\frac{dR}{dt} &= r_1IA+r_2QA+r_3HA-dR,\\
\frac{dA}{dt} &= u_3\omega+\gamma(I+Q+H)-\theta A.
\end{aligned} \tag{16}$$

To derive the optimal control functions $u_1(t), u_2(t), u_3(t)$, we use Pontryagin's maximum principle. We define the objective functional as

$$J(u_1,u_2,u_3)=\int_0^T\left[C_1I(t)+C_2Q(t)+C_3H(t)+\frac{1}{2}(B_1u_1^2+B_2u_2^2+B_3u_3^2)\right]dt.$$

We aim to minimize the number of infected individuals and the cost of applying controls. We construct the Hamiltonian as

$$\begin{aligned}\mathcal{H} = {} & C_1 I + C_2 Q + C_3 H + \frac{1}{2}(B_1 u_1^2 + B_2 u_2^2 + B_3 u_3^2) \\ & + \xi_1 \left(\Pi - \frac{\lambda S I}{1+A} - dS\right) \\ & + \xi_2 \left(\frac{\lambda S I}{1+A} - \mu E - dE\right) \\ & + \xi_3 \left(\mu E - (d + \delta + qA + u_1 r_1 A) I\right) \\ & + \xi_4 \left(qIA - (d+\delta)Q - u_2 hQA - u_1 r_2 QA\right) \\ & + \xi_5 \left(u_2 hQA - (d+\delta)H - u_1 r_3 HA\right) \\ & + \xi_6 \left(r_1 IA + r_2 QA + r_3 HA - dR\right) \\ & + \xi_7 \left(u_3 \omega + \gamma(I + Q + H) - \theta A\right),\end{aligned}$$

where $\xi_i(t)$ are the adjoint variables corresponding to the state variables S, E, I, Q, H, R, A. For each state variable x_i, the adjoint equation is:

$$\frac{d\xi_i}{dt} = -\frac{\partial \mathcal{H}}{\partial x_i}, \quad \xi_i(T) = 0. \tag{17}$$

7.1. Characterize the optimal controls

To find the optimal controls, according to the maximum principle [31], set the partial derivatives of the Hamiltonian with respect to each control to zero:

For u_1, the following is determined:

$$\frac{\partial \mathcal{H}}{\partial u_1} = B_1 u_1 - \xi_3 r_1 AI - \xi_4 r_2 AQ - \xi_5 r_3 AH = 0.$$

This gives

$$u_1^* = \frac{1}{B_1}\left(\xi_3 r_1 AI + \xi_4 r_2 AQ + \xi_5 r_3 AH\right). \tag{18}$$

Solving for u_2, we get

$$\frac{\partial \mathcal{H}}{\partial u_2} = B_2 u_2 - \xi_4 hQA + \xi_5 hQA = 0.$$

This again gives

$$u_2^* = \frac{hQA}{B_2}(\xi_4 - \xi_5). \tag{19}$$

Finally, solving for u_3, we get

$$\frac{\partial \mathcal{H}}{\partial u_3} = B_3 u_3 - \xi_7 \omega = 0,$$

which gives

$$u_3^* = \frac{\xi_7 \omega}{B_3}. \tag{20}$$

Applying the bounds for the control functions, $0 \le u_i \le 1$), we finally write using the

$$u_i^* = \min\left(1, \max(0, u_i^*)\right), i = 1, 2, 3. \tag{21}$$

Now we derive the adjoint system. Using the Eq (17), the adjoint system is obtained as

$$\begin{aligned}
\frac{d\xi_1}{dt} &= \xi_1\left(\frac{\lambda I}{1+A}+d\right)-\xi_2\left(\frac{\lambda I}{1+A}\right),\\
\frac{d\xi_2}{dt} &= \xi_2(\mu+d)-\xi_3\mu,\\
\frac{d\xi_3}{dt} &= \xi_1\left(\frac{\lambda S}{1+A}\right)-\xi_2\left(\frac{\lambda S}{1+A}\right)+\xi_3(d+\delta+qA+u_1r_1A)-\xi_4qA-\xi_6u_1r_1A-\xi_7\gamma,\\
\frac{d\xi_4}{dt} &= \xi_4(d+\delta+hA+u_1r_2A)-\xi_5u_2hA-\xi_6r_2A-\xi_7\gamma,\\
\frac{d\xi_5}{dt} &= \xi_5(d+\delta+u_1r_3A)-\xi_6u_1r_3A-\xi_7\gamma,\\
\frac{d\xi_6}{dt} &= \xi_6d,\\
\frac{d\xi_7}{dt} &= \xi_1\left(\frac{\lambda SI}{(1+A)^2}\right)-\xi_2\left(\frac{\lambda SI}{(1+A)^2}\right)+\xi_3I(q+r_1)+\xi_4Q(u_2h+r_2)+\xi_5Hr_3-\xi_7\theta.
\end{aligned} \tag{22}$$

The optimal system contains the state system (16), adjoint system (22), and the optimal controls in (21). The state system is an initial value problem, the adjoint system is a boundary value problem with boundary conditions $\xi_i(t_f) = 0$, $i = 1, 2, ..., 7$, and t_f is the final time of the optimal control problem.

8. Numerical results

In this section, we study the behaviors of the infectious disease using the analytical analysis of the proposed model presented in the previous sections. Results are presented using the following figures and discussed using biological implications.

In Figure 3, the sensitivity indices of the parameters are plotted. We identify the main parameters from this figure. Infection rate λ and recruitment rate Π are responsible for the disease, whereas the treatment rate r_1, quarantine rate q, and awareness campaign rate ω are useful for disease management.

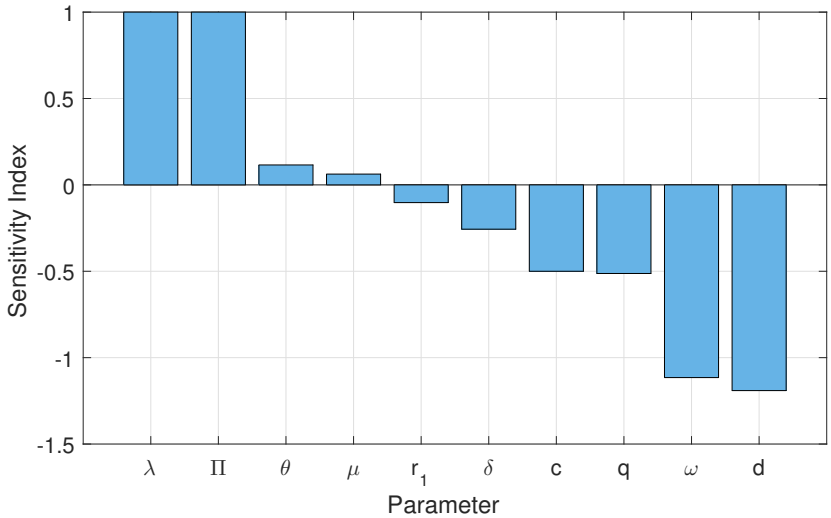

Figure 3. Sensitivity indices of parameters are plotted using their values from Table 1.

The region of stability of the DFE is shown in different parameter planes (see Figure 4). The existence and stable region of the endemic equilibrium is also observed in this figure. Region of stability ofE_0 increases when infection rate is lower and treatment is higher. Disease can be eradicated by using awareness-based control measures.

In Figure 2, we plotted the steady states values of the infected population with respect to the basic reproduction number, R_0. Forward bifurcation between disease-free and endemic equilibrium. When $R_0 < 1$, we found that the DFE is stable and endemic equilibrium exists when $R_0 > 1$. If we can reduce the infection rate, the disease can be eradicated. This can be done using awareness campaigns, i.e., increasing the rate of awareness campaign, ω.

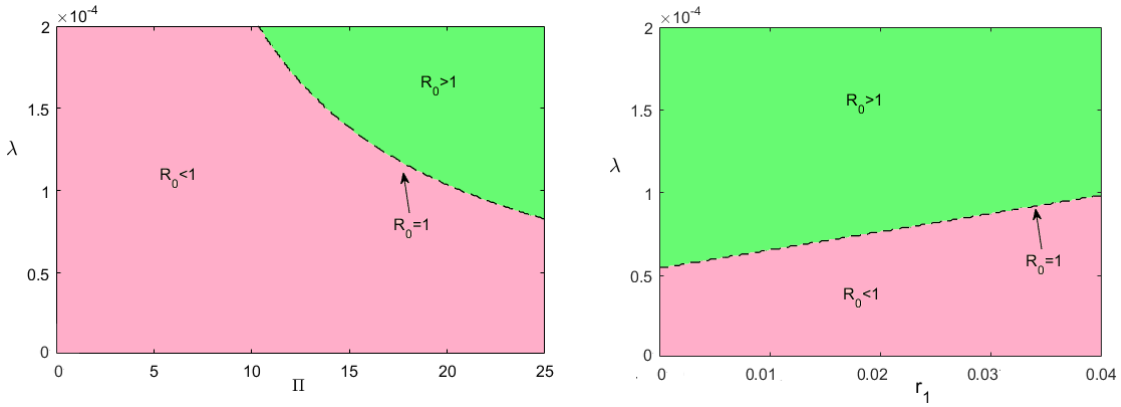

Figure 4. Regions of stability in $\Pi - \lambda$ and $r_1 - \lambda$ parameter planes. Other parameter values are taken from Table 1.

In Figure 5, we plotted the numerical solutions of the system without control for two different values of the infection rate, λ. Higher infection rate creates oscillations in the system. It that case, we have to increase the control measures such as hospitalization rate, treatment rate, to reduce infection rate. Figure 6 represents the bifurcation diagram for λ. A bubbling type dynamics has been observed in the system. That means if the value of λ increases, Hopf bifurcation occurs and further increments in λ; the Hopf bifurcation limit cycles disappeared and stable endemic equilibrium can be seen again. We have also seen that the system remains stable and endemic for more higher values of infection rate.

Impact of hospitalization is shown in Figures 7 and 8. These figures indicate that periodic oscillation, i.e., Hopf bifurcation, can be controlled using higher rate of hospitalization but disease can not be eradicated using hospitalization only. Role of awareness campaign rate is studied in Figure 9. For higher awareness campaign rate, diseased-populations go to extinction. This shows that awareness campaigns through media can help in reducing the infection, and ultimately by treatment methods the disease can be eradicated as indicated by the figure.

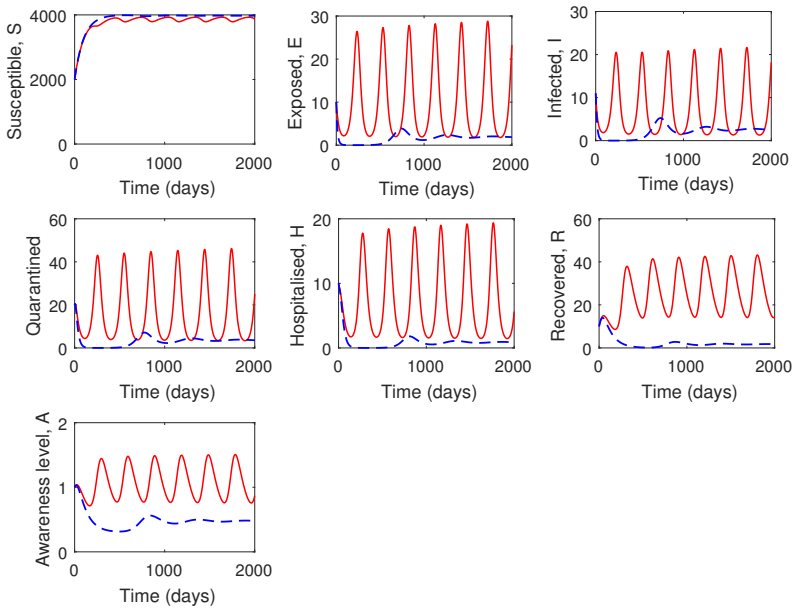

Figure 5. Numerical solutions of the system (1) are shown using the parameter values as in Figure 3 except $\lambda = 0.00003$ (blue lines), $\lambda = 0.00007$ (red lines). Here, we took $h = 0.02, \omega = 0.003$.

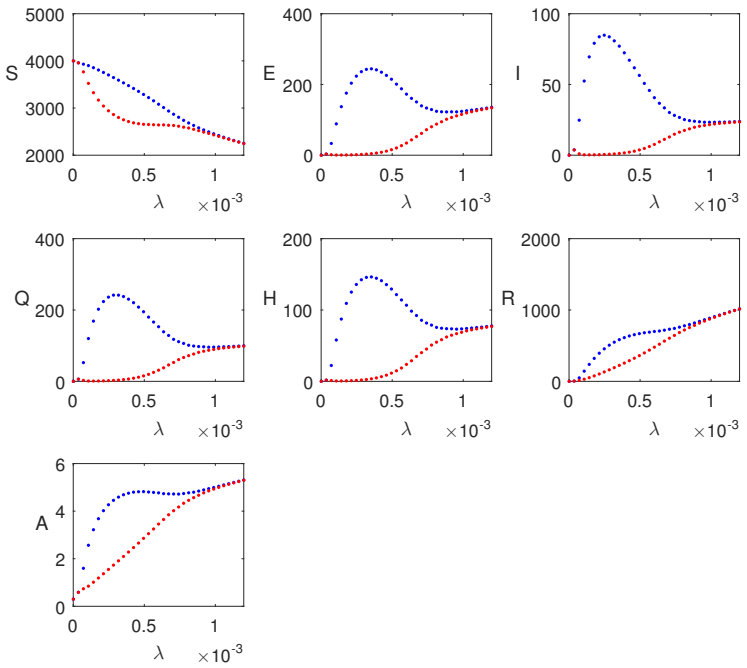

Figure 6. Hopf bifurcation diagram of the endemic equilibrium taking infection rate λ as the bifurcation parameter. The set of parameters is the same as in Figure 2.

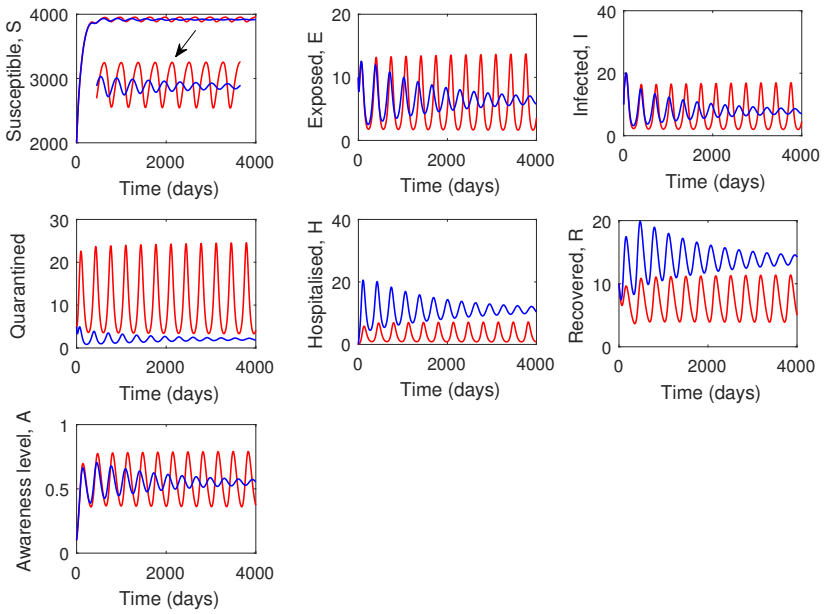

Figure 7. Numerical solutions of the system (1) are shown using the parameter values as in Figure 3 except h. Red lines are for $h = 0.01$, and blue lines are for $h = 0.2$. $\lambda = 0.00003, \Pi = 40, d = 0.01, \mu = 0.12, \delta = 0.02, q = 0.12, r_1 = 0.003, r_2 = 0.003, r_3 = 0.02, \gamma = 0.00025, \theta = 0.01, c = 0.5$.

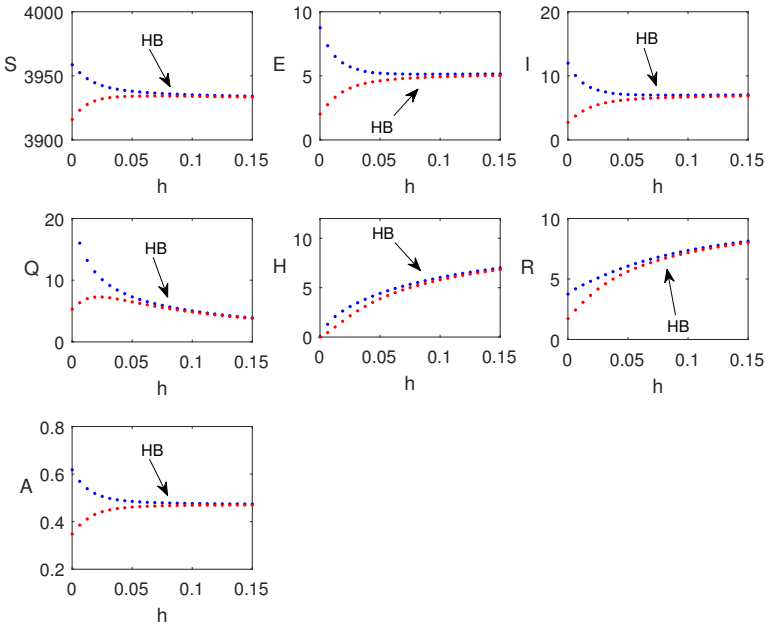

Figure 8. Bifurcation diagram of h is plotted using parameter values as in Figure 7.

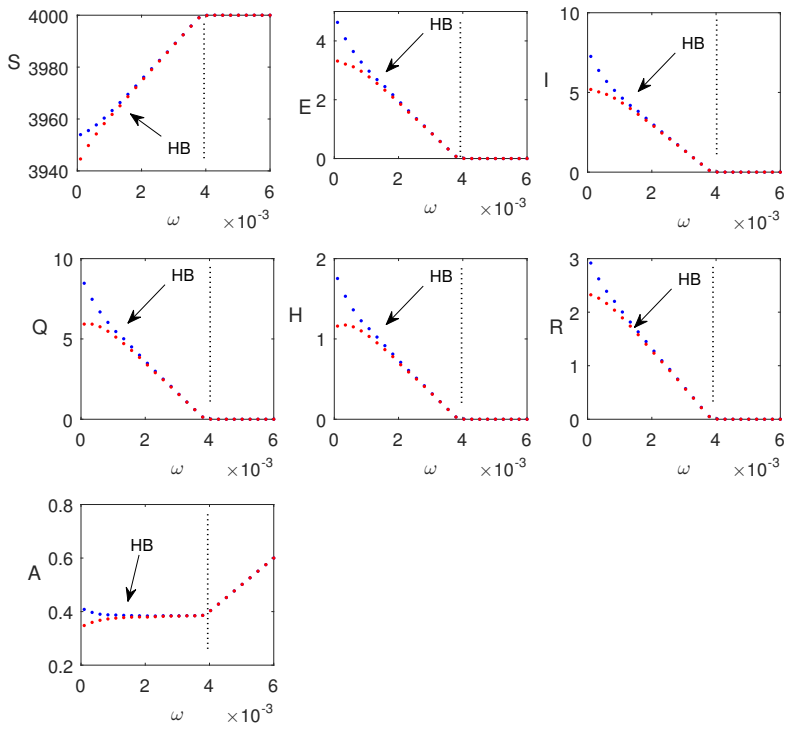

Figure 9. Bifurcation diagram of ω is plotted for $\lambda = 0.000025, h = 0.02$, and the rest of the parameters are from Figure 8.

8.1. Results from the optimal control problem

To numerically solve the optimal control problem, we employ the forward-backward sweep method, which is well-suited for systems governed by differential equations with optimality conditions. The complete optimality system comprises three components: The state equations, which are integrated forward in time from the initial conditions; the adjoint equations, which are integrated backward in time from the terminal conditions; and the optimal control characterizations, which provide explicit expressions for the control variables in terms of the state and adjoint variables. The numerical procedure begins with an initial guess for the control functions $u_1(t)$ and $u_2(t)$ over the time interval $[0, t_f]$. Using these initial controls, the state equations are solved forward in time using a suitable numerical integration method, such as the fourth-order Runge-Kutta scheme. The resulting state trajectories are then used to solve the adjoint equations backward in time, again using an appropriate numerical method. With the updated state and adjoint variables, the control functions are recalculated using the optimality conditions and projected onto the admissible control set, typically the interval $[0, 1]$. This process is repeated iteratively, updating the controls at each step, until convergence is achieved—typically when successive iterations yield negligible changes in the control profiles or the value of the objective functional. This iterative scheme ensures consistency between the state, adjoint, and control variables, thereby yielding an optimal solution to the control problem.

In Figure 10, we plotted the simulations of the optimal state system and also compared the results graphically with the system without control. We have seen that controls triplets have significant impact

on the infected populations. Infected peoples decreased significantly and the healthy peoples increased using the control approach.

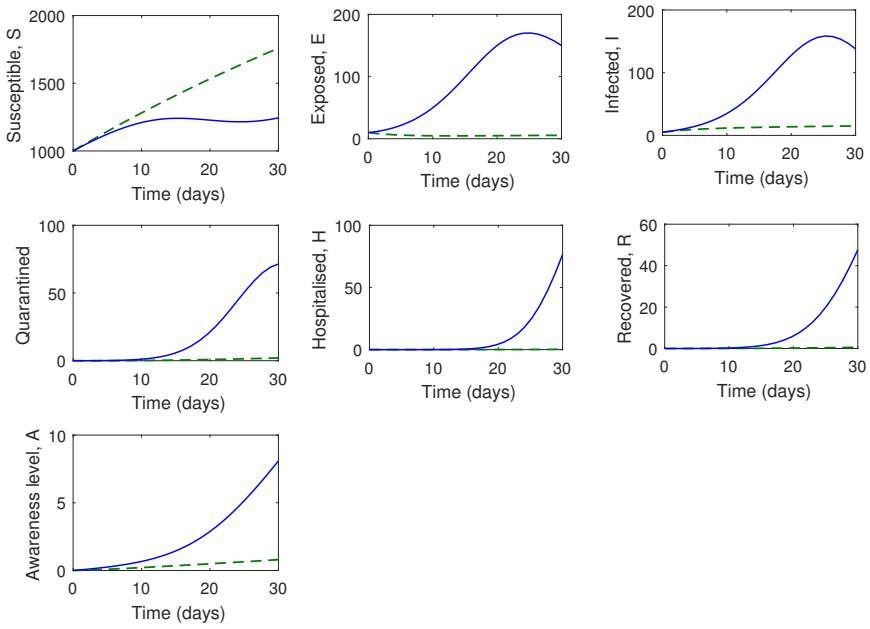

Figure 10. State system is plotted using the parameter values as in Table 1. Blue solid lines represent the solutions without control, and solutions with optimal control are given by green dashed lines.

Figure 11 shows the profiles of the optimal control functions. These results indicated that all the control measures are important for disease management. Hospitalization rate, awareness campaign rate and treatment rate should be controlled using the optimal profiles shown in this figure.

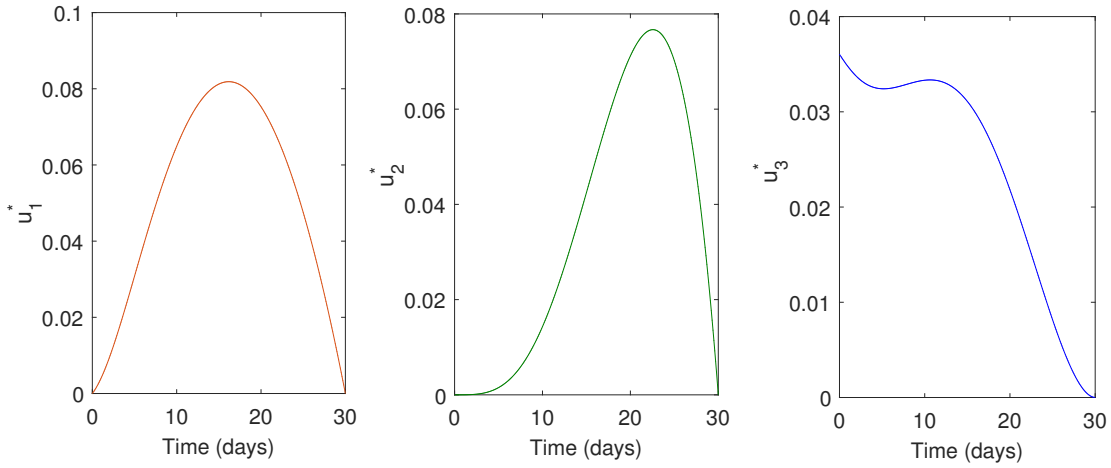

Figure 11. Control function functions are plotted as function of time. Parameter values are taken from 10.

9. Conclusions

SEIR-based models provide robust frameworks for infectious disease management. By incorporating quarantine (Q) and hospitalization dynamics (H), they offer comprehensive insights into the interplay between disease progression, public health measures, and societal behavior—ultimately contributing to more informed and effective epidemic control strategies. Here, we have developed an SEIQHR-based model, can be named as SEIQHRA model, using media awareness as an additional model population. Further, we applied optimal control theory to find optimal control on hospitalization, treatment, and awareness campaign rates for cost-minimization.

Analytically, the proposed SEIQHRA model is studied by finding the boundedness of solutions and determining the equilibria and the basic reproduction number. The stability of these equilibria is assessed in relation to the reproduction number, R_0. When $R_0 < 1$, the disease-free equilibrium remains stable, whereas for $R_0 > 1$, an endemic equilibrium arises and can be asymptotically stable under certain parameter conditions. Thus, reducing the infection rate is key to disease eradication, which may be achieved by increasing the awareness campaign rate, ω. The endemic equilibrium loses stability once the infection rate surpasses its critical threshold. Furthermore, in scenarios of high infection rates where periodic oscillations occur, the combined effects of awareness campaigns and hospitalization contribute to stabilizing the system. Moreover, we formulated an optimal control problem and solved using maximum principle and Hamiltonian function formulation. Simulations of the optimal system give the optimal control functions that control the hospitalization, treatment, and awareness campaign rates. These functions show that when the disease outbreaks, initially high rate of control measures are required, but later, gradually these can be reduced to minimize the cost.

In conclusion, the model shows how awareness can shape disease transmission and progression, making it a useful tool for studying public health measures such as media campaigns or behavioral changes. The findings can help guide strategies for managing infectious diseases. We also recognize that assuming all control rates scale linearly with awareness is a simplification. In reality, recovery, quarantine, and hospitalization rates may not increase in perfect proportion to awareness, and effects like saturation or thresholds could be more realistic. As future work, the model can be refined by including saturated infection terms when case numbers are high [29], and by exploring fractional-order approaches with real data for greater accuracy [32].

Author contributions

Khalid Alawsari: Methodology, validation, software, visualization; Fahad Al Basir: Conceptualization, methodology, validation, software, writing-original draft preparation, supervision. All authors have read and agreed to publish the manuscript.

Use of Generative-AI tools declaration

The authors declare they have not used Artificial Intelligence (AI) tools in the creation of this article.

Acknowledgments

The authors extend their appreciation to Prince Sattam bin Abdulaziz University for funding this research work through the project number (PSAU/ 2025/01/34088).

Conflict of interest

The authors declare no conflict of interest.

References

1. B. Baral, K. Mamale, S. Gairola, C. Chauhan, A. Dey, R. K. Kaundal, Infectious diseases and its global epidemiology, In: *Nanostructured drug delivery systems in infectious disease treatment*, Academic Press, 2024, 1–24. https://doi.org/10.1016/B978-0-443-13337-4.00017-3
2. J. Huang, J. S. Morris, Infectious disease modeling, *Annu. Rev. Stat. Appl.*, **12** (2025), 19–44. https://doi.org/10.1146/annurev-statistics-112723-034351
3. P. R. Kumaraswamy, S. Hameed, M. M. Quamar, *COVID-19 in Middle East and north africa: Pandemic, impacts and responses*, Bloomsbury Publishing, 2025.
4. Z. A. Memish, S. Perlman, M. D. V. Kerkhove, A. Zumla, Middle East respiratory syndrome, *Lancet*, **395** (2020), 1063–1077. https://doi.org/10.1016/S0140-6736(19)33221-0
5. K. Al-Ahmadi, S. Alahmadi, A. Al-Zahrani, Spatiotemporal clustering of Middle East respiratory syndrome coronavirus (MERS-CoV) incidence in Saudi Arabia, 2012–2019, *Int. J. Env. Res. Pub. He.*, **16** (2019), 2520. https://doi.org/10.3390/ijerph16142520
6. M. K. Hussain, M. B. Osman, An evaluation of public health surveillance system in ministry of health, Saudi Arabia, *Pac. Bus. Rev. Int.*, **18** (2025), 103–119.
7. N. K. Alhumaid, A. M. Alajmi, N. F. Alosaimi, M. Alotaibi, T. A. Almangour, M. S. Nassar, et al., Epidemiology of reportable bacterial infectious diseases in Saudi Arabia, *Infect. Dis. Ther.*, **13** (2024), 667–684. https://doi.org/10.1007/s40121-024-00942-1
8. M. A. Ryani, Hepatitis management in Saudi Arabia: Trends, prevention, and key interventions (2016–2025), *Medicina*, **61** (2025), 1509. https://doi.org/10.3390/medicina61091509
9. M. S. Aleyiydi, N. M. Alshiban, A. M. Alajmi, N. F. Alosaimi, M. Alotaibi, M. S. Nassar, et al., Epidemiology of viral infectious diseases reported in Saudi Arabia, *Infect. Dis. Ther.*, **13** (2024), 1893–1905. https://doi.org/10.1007/s40121-024-01014-0
10. J. Lamwong, P. Pongsumpun, Optimal control and stability analysis of REF12 transmission dynamics with quarantine interventions, *Model. Earth Syst. Env.*, **11** (2025), 233. https://doi.org/10.1007/s40808-025-02413-z
11. M. Navascués, C. Budroni, Y. Guryanova, Disease control as an optimization problem, *PLoS One*, **16** (2021), e0257958. https://doi.org/10.1371/journal.pone.0257958
12. F. A. Basir, B. Rajak, B. Rahman, K. Hattaf, Hopf bifurcation analysis and optimal control of an infectious disease with awareness campaign and treatment, *Axioms*, **12** (2023), 608. https://doi.org/10.3390/axioms12060608

13. D. Y. Trejos, J. C. Valverde, E. Venturino, Dynamics of infectious diseases: A review of the main biological aspects and their mathematical translation, *Appl. Math. Nonlin. Sci.*, **7** (2022).

14. Y. Kao, P. J. Chu, P. C. Chou, C. C. Chen, A dynamic approach to support outbreak management using reinforcement learning and semi-connected SEIQR models, *BMC Public Health*, **24** (2024), 751. https://doi.org/10.1186/s12889-024-18251-0

15. I. Ullah, N. Ali, I. U. Haq, I. Ahmad, M. D. Albalwi, M. H. A. Biswas, Analysis of COVID-19 disease model: Backward bifurcation and impact of pharmaceutical and nonpharmaceutical interventions, *Int. J. Math. Math. Sci.*, **2024** (2024), 6069996. https://doi.org/10.1155/2024/6069996

16. W. O. Kermack, A. G. McKendrick, A contribution to the mathematical theory of epidemics, *P. Roy. Soc. A*, **115** (1927), 700–721. https://doi.org/10.1098/rspa.1927.0118

17. H. Gaff, E. Schaefer, Optimal control applied to vaccination and treatment strategies for various epidemiological models, *Math. Biosci. Eng.*, **6** (2009), 469–492. https://doi.org/10.3934/mbe.2009.6.469

18. A. d'Onofrio, M. Iannelli, P. Manfredi, G. Marinoschi, Optimal epidemic control by social distancing and vaccination of an infection structured by time since infection: The COVID-19 case study, *SIAM J. Appl. Math.*, **84** (2024), S199–S224. https://doi.org/10.1137/22M1499406

19. W. O. Kermack, A. G. McKendrick, Contributions to the mathematical theory of epidemics, II.—The problem of endemicity, *P. Roy. Soc. A*, **138** (1932), 55–83. https://doi.org/10.1098/rspa.1932.0171

20. S. He, Y. Peng, K. Sun, SEIR modeling of the COVID-19 and its dynamics, *Nonlinear Dynam.*, **101** (2020), 1667–1680. https://doi.org/10.1007/s11071-020-05743-y

21. Y. Kao, P. J. Chu, P. C. Chou, C. C. Chen, A dynamic approach to support outbreak management using reinforcement learning and semi-connected SEIQR models, *BMC Public Health*, **24** (2024), 751. https://doi.org/10.1186/s12889-024-18251-0

22. F. Z. Younsi, A. Younsi, M. E. Mekhlouf, Understanding the SEIQR-SF epidemic model system: A comprehensive overview of disease dynamics and control strategies, *Bratisl. Med. J.*, **126** (2025), 2991–3009. https://doi.org/10.1007/s44411-025-00314-2

23. A. Abta, Optimal Control Strategies in SEIQHR Models for Epidemic Management, *Math. Biosci.*, **250** (2014), 1–12.

24. M. Xing, H. Zhan, Y. Ye, R. Lu, Dynamics and combinational optimal control of the SEIQHR epidemic model, *Preprint*, (2024), https://doi.org/10.21203/rs.3.rs-4207437/v1

25. C. Jia, X. Wang, Y. Chen, Complex dynamics of an SIHR epidemic model with variable hospitalization rate depending on unoccupied hospital beds, *Math. Comput. Simulat.*, **229** (2025), 706–724. https://doi.org/10.1016/j.matcom.2024.10.023

26. J. Maurya, K. B. Blyuss, A. K. Misra, Modeling the impact of hospital beds and vaccination on the dynamics of an infectious disease, *Math. Biosci.*, **368** (2024), 109133. https://doi.org/10.1016/j.mbs.2023.109133

27. A. Kumar, A. K. Agrawal, Existence of Hopf-bifurcation in a 6-dimensional system, *Commun. Appl. Anal.*, **21** (2017), 119–126. https://doi.org/10.12732/caa.v21i1.7

28. C. C. Chavez, B. Song, Dynamical models of tuberculosis and their applications, *Math. Biosci. Eng.*, **1** (2004), 361–404. https://doi.org/10.3934/mbe.2004.1.361

29. R. T. Alqahtani, A. Ajbar, Study of dynamics of a COVID-19 model for Saudi Arabia with vaccination rate, saturated treatment function and saturated incidence rate, *Mathematics*, **9** (2021), 3134. https://doi.org/10.3390/math9233134

30. F. A. Basir, K. S. Nisar, I. M. Alsulami, A. N. Chatterjee, Dynamics and optimal control of an extended SIQR model with protected human class and public awareness, *Eur. Phys. J. Plus*, **140** (2025), 152. https://doi.org/10.1140/epjp/s13360-025-06108-3

31. W. H. Fleming, R. W. Rishel, *Deterministic and stochastic optimal control*, Springer Science & Business Media, 2012.

32. Y. Guo, T. Li, Fractional-order modeling and optimal control of a new online game addiction model based on real data, *Commun. Nonlinear Sci.*, **121** (2023), 107221. https://doi.org/10.1016/j.cnsns.2023.107221

33. Z. N. Li, Y. L. Tang, Z. Wang, Optimal control of a COVID-19 dynamics based on SEIQR model, *Adv. Contin. Discret. M.*, **2025** (2025), 50. https://doi.org/10.1186/s13662-025-03869-0

34. S. Tyagi, S. Gupta, S. Abbas, K. P. Das, B. Riadh, Analysis of infectious disease transmission and prediction through SEIQR epidemic model, *Nonauton. Dyn. Syst.*, **8** (2021), 75–86. https://doi.org/10.1515/msds-2020-0126

35. N. Avinash, G. B. A. Xavier, A. Alsinai, H. Ahmed, V. R. Sherine, P. Chellamani, Dynamics of COVID-19 using SEIQR epidemic model, *J. Math.*, **2022** (2022), 2138165. https://doi.org/10.1155/2022/2138165

36. T. Hussain, M. Ozair, F. Ali, S. U Rehman, T. A. Assiri, E. E. Mahmoud, Sensitivity analysis and optimal control of COVID-19 dynamics based on SEIQR model, *Results Phys.*, **22** (2021), 103956. https://doi.org/10.1016/j.rinp.2021.103956

37. K. Umapathy, B. Palanivelu, R. Jayaraj, D. Baleanu, P. B. Dhandapani, On the decomposition and analysis of novel simultaneous SEIQR epidemic model, *AIMS Math.*, **8** (2023), 5918–5933. https://doi.org/10.3934/math.2023298

38. , N. Tuncer, A. Timsina, M. Nuno, G. Chowell, M. Martcheva, Parameter identifiability and optimal control of an SARS-CoV-2 model early in the pandemic, *J. Biol. Dynam.*, **1**6 (2022), 412–438. https://doi.org/10.1080/17513758.2022.2078899

39. Y. Li, L. W. Wang, Z. H. Peng, H. B. Shen, Basic reproduction number and predicted trends of coronavirus disease 2019 epidemic in the mainland of China, *Infect. Dis. Poverty*, **9** (2020), 94. https://doi.org/10.1186/s40249-020-00704-4

Appendix A

The coefficients are given below as

$$
\begin{aligned}
J_1 =& -J_{11}-J_{22}-J_{33}-J_{44}-J_{55}-J_{77},\\
J_2 =& J_{11}J_{22}-J_{23}J_{32}+J_{11}J_{33}+J_{22}J_{33}\\
&+J_{11}(J_{44}+J_{55}+J_{77})+J_{22}(J_{44}+J_{55}+J_{77})+J_{33}(J_{44}+J_{55}+J_{77})\\
&+J_{44}J_{55}-J_{37}J_{73}-J_{47}J_{74}-J_{57}J_{75},\\
J_2 =& J_{11}J_{22}-J_{23}J_{32}+J_{11}J_{33}+J_{22}J_{33}\\
&+(J_{11}+J_{22}+J_{33})(J_{44}+J_{55}+J_{77})+J_{44}J_{55}-J_{37}J_{73}-J_{47}J_{74}-J_{57}J_{75},\\
J_3 =& J_{32}\Big[-J_{13}J_{21}+J_{11}J_{23}+J_{23}J_{44}+J_{23}J_{55}-J_{27}J_{73}+J_{23}J_{77}\Big]\\
&+J_{11}\Big[-J_{22}J_{33}-J_{22}J_{44}-J_{33}J_{44}-J_{22}J_{55}-J_{33}J_{55}-J_{44}J_{55}\\
&\quad+J_{37}J_{73}+J_{47}J_{74}+J_{57}J_{75}-J_{22}J_{77}-J_{33}J_{77}-J_{44}J_{77}-J_{55}J_{77}\Big]\\
&+J_{22}\Big[J_{37}J_{73}+J_{47}J_{74}+J_{57}J_{75}-J_{33}J_{44}-J_{33}J_{55}-J_{44}J_{55}-J_{33}J_{77}-J_{44}J_{77}-J_{55}J_{77}\Big]\\
&+J_{33}\Big[J_{47}J_{74}+J_{57}J_{75}-J_{44}J_{77}-J_{55}J_{77}\Big]\\
&+J_{37}\Big[J_{44}J_{73}+J_{55}J_{73}-J_{43}J_{74}\Big]+J_{47}\Big[J_{55}J_{74}-J_{54}J_{75}\Big]+J_{57}J_{44}J_{75},
\end{aligned}
$$

$$
\begin{aligned}
J_4 =& J_{32}J_{44}\Big[J_{13}J_{21}-J_{11}J_{23}+J_{11}J_{22}J_{33}\Big]+J_{32}J_{55}\Big[J_{13}J_{21}-J_{11}J_{23}+J_{11}J_{22}J_{33}\Big]\\
&+J_{44}J_{55}\Big[J_{11}J_{22}-J_{23}J_{32}+J_{11}J_{33}+J_{22}J_{33}\Big]+J_{32}J_{73}\Big[-J_{17}J_{21}+J_{11}J_{27}-J_{11}J_{22}J_{37}\Big]\\
&+J_{44}J_{73}\Big[J_{27}J_{32}-J_{11}J_{37}-J_{22}J_{37}\Big]+J_{55}J_{73}\Big[J_{27}J_{32}-J_{11}J_{37}-J_{22}J_{37}-J_{37}J_{44}\Big]\\
&+J_{43}J_{74}\Big[-J_{27}J_{32}+J_{11}J_{37}+J_{22}J_{37}\Big]+J_{47}J_{74}\Big[-J_{11}J_{22}+J_{23}J_{32}-J_{11}J_{33}-J_{22}J_{33}\Big]\\
&+J_{43}J_{55}J_{74}\Big[J_{37}\Big]-J_{11}J_{47}J_{55}J_{74}-J_{22}J_{47}J_{55}J_{74}-J_{33}J_{47}J_{55}J_{74}\\
&+J_{43}J_{54}J_{75}\Big[-J_{37}\Big]+J_{11}J_{47}J_{54}J_{75}+J_{22}J_{47}J_{54}J_{75}+J_{33}J_{47}J_{54}J_{75}\\
&+J_{57}J_{75}\Big[-J_{11}J_{22}+J_{23}J_{32}-J_{11}J_{33}-J_{22}J_{33}-J_{11}J_{44}-J_{22}J_{44}-J_{33}J_{44}\Big]\\
&+J_{32}J_{77}\Big[J_{13}J_{21}-J_{11}J_{23}+J_{11}J_{22}J_{33}\Big]\\
&+J_{44}J_{77}\Big[J_{11}J_{22}-J_{23}J_{32}+J_{11}J_{33}+J_{22}J_{33}\Big]\\
&+J_{55}J_{77}\Big[J_{11}J_{22}-J_{23}J_{32}+J_{11}J_{33}+J_{22}J_{33}\Big]\\
&+J_{44}J_{55}J_{77}\Big[J_{11}+J_{22}+J_{33}\Big],
\end{aligned}
$$

$$
\begin{aligned}
J_5 = {} & J_{32}J_{44}J_{55}\Big[-J_{13}J_{21}+J_{11}J_{23}-J_{11}J_{22}J_{33}\Big]+J_{32}J_{44}J_{73}\Big[J_{17}J_{21}-J_{11}J_{27}+J_{11}J_{22}J_{37}\Big]\\
& +J_{32}J_{55}J_{73}\Big[J_{17}J_{21}-J_{11}J_{27}+J_{11}J_{22}J_{37}\Big]+J_{44}J_{55}J_{73}\Big[-J_{27}J_{32}+J_{11}J_{37}+J_{22}J_{37}\Big]\\
& +J_{32}J_{43}J_{74}\Big[-J_{17}J_{21}+J_{11}J_{27}-J_{11}J_{22}J_{37}\Big]+J_{32}J_{47}J_{74}\Big[J_{13}J_{21}-J_{11}J_{23}+J_{11}J_{22}J_{33}\Big]\\
& +J_{43}J_{55}J_{74}\Big[J_{27}J_{32}-J_{11}J_{37}-J_{22}J_{37}\Big]+J_{47}J_{55}J_{74}\Big[J_{11}J_{22}-J_{23}J_{32}+J_{11}J_{33}+J_{22}J_{33}\Big]\\
& +J_{43}J_{54}J_{75}\Big[-J_{27}J_{32}+J_{11}J_{37}+J_{22}J_{37}\Big]+J_{47}J_{54}J_{75}\Big[-J_{11}J_{22}+J_{23}J_{32}-J_{11}J_{33}-J_{22}J_{33}\Big]\\
& +J_{32}J_{57}J_{75}\Big[J_{13}J_{21}-J_{11}J_{23}+J_{11}J_{22}J_{33}\Big]+J_{44}J_{57}J_{75}\Big[J_{11}J_{22}-J_{23}J_{32}+J_{11}J_{33}+J_{22}J_{33}\Big]\\
& +J_{32}J_{44}J_{77}\Big[-J_{13}J_{21}+J_{11}J_{23}-J_{11}J_{22}J_{33}\Big],
\end{aligned}
$$

$$
\begin{aligned}
J_6 = {} & J_{32}J_{44}J_{55}\Big[-J_{17}J_{21}J_{73}+J_{11}J_{27}J_{73}-J_{11}J_{22}J_{37}J_{73}+J_{13}J_{21}J_{77}-J_{11}J_{23}J_{77}+J_{11}J_{22}J_{33}J_{77}\Big]\\
& +J_{32}J_{43}J_{55}\Big[J_{17}J_{21}J_{74}-J_{11}J_{27}J_{74}+J_{11}J_{22}J_{37}J_{74}-J_{17}J_{21}J_{75}+J_{11}J_{27}J_{75}-J_{11}J_{22}J_{37}J_{75}\Big]\\
& +J_{32}J_{47}J_{55}\Big[-J_{13}J_{21}J_{74}+J_{11}J_{23}J_{74}-J_{11}J_{22}J_{33}J_{74}\Big]\\
& +J_{32}J_{47}J_{54}\Big[J_{13}J_{21}J_{75}-J_{11}J_{23}J_{75}+J_{11}J_{22}J_{33}J_{75}\Big]\\
& +J_{32}J_{44}J_{57}\Big[-J_{13}J_{21}J_{75}+J_{11}J_{23}J_{75}-J_{11}J_{22}J_{33}J_{75}\Big].
\end{aligned}
$$

AIMS Press